journal

J. Am. Ceram. Soc., 91 [6] 1835–1844 (2008)
DOI: 10.1111/j.1551-2916.2008.02413.x

Phase-Field Method of Phase Transitions/Domain Structures in Ferroelectric Thin Films: A Review

Long-Qing Chen†

Department of Materials Science and Engineering and Materials Research Institute, the Pennsylvania State University, University Park, Pennsylvania 16802

This article briefly reviews recent applications of phase-field method to ferroelectric phase transitions and domain structures in thin films. It starts with a brief introduction to the thermodynamics of coupled electromechanical systems and the Landau description of ferroelectric transitions in homogeneous ferroelectric single crystals. The thermodynamic potentials of a homogeneous crystal under different mechanical boundary conditions are presented, including the thin-film boundary conditions. The phase-field approach to inhomogeneous systems containing domain structures is then outlined. It describes a domain structure using the spatial distribution of spontaneous polarization. The evolution of a domain structure towards equilibrium is driven by the reduction in the total-free energy of an inhomogeneous domain structure including the chemical driving force, domain wall energy, electrostatic energy as well as elastic energy. A number of examples are discussed, including phase transitions and domain stability in ferroelectric thin films and superlattices. It is demonstrated that using a set of independently measured thermodynamic parameters for the corresponding bulk single crystals, the phase-field approach is able to quantitatively predict not only the strain effect on phase transition temperatures but also the correct ferroelectric domain structures for a given strain and temperature.

I. Introduction

Ferroelectrics, discovered in 1921, are a family of materials possessing a spontaneous polarization that can be switched between crystallographically equivalent states in a single crystal by an electric field. One of the common features for ferroelectrics is the formation of domain structures when a paraelectric phase is cooled through the ferroelectric transition temperature. For example, in a cubic to tetragonal transformation, there are six possible domains with the spontaneous polarization along or opposite to the [100], [010], and [001] directions of the cubic paraelectric phase. In the absence of any external field or constraint, they are energetically degenerate, and thus all of them have the same probability of forming in a parent phase below the ferroelectric transition temperature. The corresponding domain structure of the ferroelectric phase will contain all possible orientations of domains with approximately equal volume fractions, separated by the so-called domain walls. The fundamental understanding of the stability of domains and their responses to external electric field is critical for many applications of ferroelectrics.

As all ferroelectric phase transitions are accompanied by a change in the crystal structure and thus the lattice parameters, domain configurations in ferroelectrics could be drastically changed by external constraints. For example, for ferroelectric thin films constrained by a substrate, strain can significantly affect both the Curie temperature and the relative volume fractions of domains with different polarization directions (see, e.g., a recent review[1]). It has been shown that the phenomenological thermodynamics based on the Landau–Devonshire theory can provide remarkably good predictions on the strain effects on ferroelectric phase transition temperatures,[2–4] provided that reliable thermodynamic potential functions are available.

Analytical thermodynamic theories, however, typically assume a homogeneous paraelectric state transforming to a homogeneous single-domain ferroelectric phase, i.e., all the order parameters including strain are assumed to be spatially homogeneous. In the absence of significant built-in bias field, a ferroelectric thin film is rarely uniform, i.e., it almost always contains domain structures. In a domain structure, both the polarization field and the strain field are inhomogeneous, and the total free energy of a thin film is a functional of all the spatially dependent order parameters, i.e., domain structure is an internal variable with respect to which the total-free energy has to be minimized. Indeed, it has been shown that different assumptions of the domain state of a thin film in the thermodynamic theory may lead to fundamentally different domain stability diagrams.[2,5,6]

The focus of this article is to provide a brief review of thermodynamics and the phase-field method as they are applied to the study of strain effect on phase transitions and domain structures. It starts with a brief review of the thermodynamics for coupled electromechanical systems, followed by the Landau description of ferroelectric transitions for bulk single crystals. Thermodynamic theory of ferroelectric phase transitions under various mechanical boundary conditions will be discussed, including the thin-film boundary condition and the effect of a substrate strain on the transition temperatures and ferroelectricity. A number of recent examples of applying the phase-field method to ferroelectric thin films are then presented, including $PbTiO_3$, $BaTiO_3$, $PbZr_xTi_{1-x}O_3$ (PZT), $BiFeO_3$ thin films and $BaTiO_3/SrTiO_3$ superlattices.

(1) Thermodynamics of Coupled Electromechanical Systems

In a classical description of thermodynamics, the combined first and second law of thermodynamics is given by

$$dU = TdS + \sigma_{ij}d\varepsilon_{ij} + E_i dD_i \quad (1)$$

where T is temperature, S is entropy, σ_{ij} is a component of the second-rank stress tensor, ε_{ij} is the corresponding component of the strain tensor, E_i and D_i are ith components of electric field and electric displacement, respectively, and, i and j run from one to three. In this paper, the Einstein convention is used, i.e., repeated indices in a given term imply summation over the corresponding indices. In most experimental measurements, it is more convenient to use thermodynamic potentials other than the internal energy. For example, if the desirable independent

Q. X. Jia—contributing editor

Manuscript No. 23935. Received November 5, 2007; approved January 1, 2008.
Article was invited by guest editors from the Electronics Division.
The author is grateful for the financial support from NSF under the grant numbers DMR0122638 and DMR-0507146, and DOE DE-FG02-07ER46417.
†Author to whom correspondence should be addressed. e-mail: lqc3@psu.edu

variables are T, σ_{ij}, and E_i, the corresponding thermodynamic function is the Gibbs-free energy and its differential form is

$$dG = -SdT - \varepsilon_{ij}d\sigma_{ij} - D_i dE_i \quad (2)$$

To incorporate the strain contribution to the thermodynamics of ferroelectric phase transitions, it is usually more convenient to choose strain and polarization (P_i) as independent variables. The appropriate thermodynamic potential for this set of independent variables is then the Helmholtz-free energy, $F = F(\varepsilon_{ij}, P_i)$. Assuming isothermal, its differential form is given by

$$dF = \sigma_{ij}d\varepsilon_{ij} + E_i dP_i \quad (3)$$

For most of the discussions in this article, including the effect of different mechanical boundary conditions and the phase-field method, we use the Helmholtz-free energy for the description of thermodynamics.

(2) Phenomenological Description of Ferroelectric Phase Transitions

Using the free energy for the unpolarized and unstrained crystal as the reference, one can write down the free energy as a function of strain and polarization using the Landau–Devinshire theory of ferroelectrics[7]

$$\begin{aligned} F(\varepsilon, P) = {} & \tfrac{1}{2}\alpha_{ij}P_iP_j + \tfrac{1}{3}\beta_{ijk}P_iP_jP_k + \tfrac{1}{4}\gamma_{ijkl}P_iP_jP_kP_l \\ & + \tfrac{1}{5}\delta_{ijklm}P_iP_jP_kP_lP_m + \tfrac{1}{6}\omega_{ijklmn}P_iP_jP_kP_lP_mP_n \\ & + \cdots + \tfrac{1}{2}c_{ijkl}\varepsilon_{ij}\varepsilon_{kl} - a_{ijk}\varepsilon_{ij}P_k - \tfrac{1}{2}q_{ijkl}\varepsilon_{ij}P_kP_l \end{aligned} \quad (4)$$

where α_{ij}, β_{ijk}, γ_{ijkl}, δ_{ijklm} and ω_{ijklmn} are the phenomenological Landau expansion coefficients, c_{ijkl}, a_{ijk} and q_{ijkl} are the elastic, piezoelectric, and electrostrictive constant tensors, respectively. All the coefficients are generally assumed to be constant except α_{ij} which is linearly proportional to temperature, i.e., $\alpha_{ij} = \alpha^o_{ij}(T - T_o)$, where T_o is the Curie temperature. If the parent phase is centrosymmetric, all odd terms are absent,

$$\begin{aligned} F(\varepsilon, P) = {} & \tfrac{1}{2}\alpha_{ij}P_iP_j + \tfrac{1}{4}\gamma_{ijkl}P_iP_jP_kP_l + \tfrac{1}{6}\omega_{ijklmn}P_iP_jP_kP_lP_mP_n \\ & + \ldots + \tfrac{1}{2}c_{ijkl}\varepsilon_{ij}\varepsilon_{kl} - \tfrac{1}{2}q_{ijkl}\varepsilon_{ij}P_kP_l \end{aligned} \quad (5)$$

(3) Spontaneous Polarization and Strains in Ferroelectric Phase Transitions

The spontaneous polarization at zero strain at a temperature below the ferroelectric phase transition is given by the solution to the equation,

$$\frac{\partial F(\varepsilon = 0, P)}{\partial P} = 0 \quad (6)$$

The spontaneous strain is the crystal shape deformation caused by a phase transformation under a stress-free condition. The stress is given by

$$\sigma_{ij} = \left(\frac{\partial F}{\partial \varepsilon_{ij}}\right)_{T, P_k} \quad (7)$$

or

$$\sigma_{ij} = c_{ijkl}\varepsilon_{kl} - a_{ijk}P_k - \tfrac{1}{2}q_{ijkl}P_kP_l \quad (8)$$

The spontaneous strain is then given by $\sigma_{ij} = 0$, i.e.,

$$\varepsilon^o_{ij}(P_k) = \tfrac{1}{2}s_{ijmn}q_{mnkl}P_kP_l = Q_{ijkl}P_kP_l \quad (9)$$

where Q_{ijkl} are the electrostrictive coefficients measured experimentally. The corresponding spontaneous polarization at zero stress can be found using the spontaneous strain (9) in (5) and then find the polarization that minimizes the Landau-free energy. The electrostrictive coefficients, q_{ijkl}, defined in the Helmholtz-free energy, can be easily obtained from Q_{ijkl} through

$$q_{ijkl} = 2c_{ijmn}Q_{mnkl} \quad (10)$$

It should be emphasized that spontaneous strain is not an elastic strain, and it is rather a plastic strain. For a typical proper cubic to tetragonal ferroelectric phase transformation in perovskites, the stress-free strain in terms of the unit cell dimensions of the cubic and tetragonal phases (Fig. 1) is given by

$$\varepsilon^o_{ij} = \begin{bmatrix} (a_t - a_c)/a_c & 0 & 0 \\ 0 & (a_t - a_c)/a_c & 0 \\ 0 & 0 & (c - a_c)/a_c \end{bmatrix}$$

where a_c is the lattice parameter of the cubic phase, and a_t and c are the a and c lattice parameters of the tetragonal phase, respectively, both under stress-free conditions.

(4) Strain Contribution Under Different Mechanical Boundary Conditions

The strain contributions to the ferroelectric phase transitions depend on the type of mechanical boundary conditions as materials properties vary under different thermodynamic conditions. For simplicity, let us assume that the polarization direction for a single domain state is (0, 0, P_3), and the paraelectric crystal is centrosymmetric. The Helmholtz-free energy up to six-order terms is then reduced to

$$\begin{aligned} F(\varepsilon, P_3) = {} & \tfrac{1}{2}\alpha P_3^2 + \tfrac{1}{4}\gamma P_3^4 + \tfrac{1}{6}\omega P_3^6 + \tfrac{1}{2}c_{ijkl}\varepsilon_{ij}\varepsilon_{kl} \\ & - \tfrac{1}{2}q_{ij33}\varepsilon_{ij}P_3^2 \end{aligned} \quad (11)$$

(A) Clamped Boundary Condition: For a clamped boundary condition, the crystal as a whole is not allowed to deform. Therefore, the strain is zero, and the free energy becomes

$$F(\varepsilon = 0, P_3) = \tfrac{1}{2}\alpha P_3^2 + \tfrac{1}{4}\gamma P_3^4 + \tfrac{1}{6}\omega P_3^6 \quad (12)$$

i.e., the set of coefficients, α, γ, and ω in the Helmholtz-free energy correspond to those measured at zero strain. Under this condition, the ferroelectric crystal is stressed, and the magnitude of the stress can be readily calculated through the free energy dependence on strain through

$$\sigma_{ij} = \left(\frac{\partial F}{\partial \varepsilon_{ij}}\right)_{P_i, \varepsilon_{ij}=0} = -\tfrac{1}{2}q_{ij33}P_3^2 \quad (13)$$

which shows that the stress is zero before the transformation, and its magnitude increases with polarization quadratically in the ferroelectric state.

(B) Constant Applied Strain: This is very similar to the zero strain condition. Assuming that the paraelectric crystal is

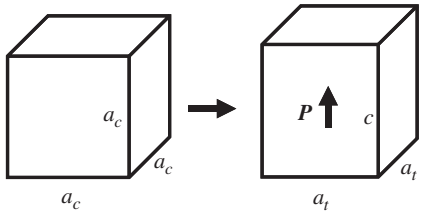

Fig. 1. Illustration of a cubic unit cell transformed to a tetragonal cell with polarization along the [001] direction.

prestrained, the free energy is given by

$$F(\varepsilon^a, P_3) = \tfrac{1}{2}\alpha P_3^2 + \tfrac{1}{4}\gamma P_3^4 + \tfrac{1}{6}\omega P_3^6 + \tfrac{1}{2}c_{ijkl}\varepsilon_{ij}^a\varepsilon_{kl}^a - \tfrac{1}{2}q_{ij33}\varepsilon_{ij}^a P_3^2 \quad (14)$$

where ε^a is the magnitude of an applied strain. Combining the two second-order terms in P_3 in the free energy expression (14), we have

$$F(\varepsilon^a, P_3) = \tfrac{1}{2}\left(\alpha - q_{ij33}\varepsilon_{ij}^a\right)P_3^2 + \tfrac{1}{4}\gamma P_3^4 + \tfrac{1}{6}\omega P_3^6 + \tfrac{1}{2}c_{ijkl}\varepsilon_{ij}^a\varepsilon_{kl}^a \quad (15)$$

If

$$\alpha = \alpha_1(T - T_o) \quad (16)$$

where T_o is the Curie–Weiss temperature under the clamped boundary condition, the Curie–Weiss temperature under a constant applied strain is given by

$$T_o' = T_o + \frac{q_{ij33}\varepsilon_{ij}^a}{\alpha_1} \quad (17)$$

The stress in the crystal under a constant applied strain depends on both the magnitude of the applied strain and the value of the polarization

$$\sigma_{ij} = \left(\frac{\partial F}{\partial \varepsilon_{ij}}\right)_{P_i, \varepsilon_{ij}=\varepsilon_{ij}^a} = c_{ijkl}\varepsilon_{kl}^a - \tfrac{1}{2}q_{ij33}P_3^2 \quad (18)$$

(C) Stress-Free Boundary Condition: Under the stress-free boundary condition, the macroscopic shape change of a crystal due to the ferroelectric phase transition is described by the spontaneous strain which can be obtained through the derivative of the Helmholtz-free energy (11) with respect to strain, i.e.,

$$\sigma_{ij} = c_{ijkl}\varepsilon_{kl} - \tfrac{1}{2}q_{ij33}P_3^2 = 0 \quad (19)$$

Solving Eq. (19) for strain, we have,

$$\varepsilon_{ij} = \tfrac{1}{2}s_{ijkl}q_{kl33}\ P_3^2 \quad (20)$$

Substituting the spontaneous strain (20) back to the free energy expression (11), one gets

$$F(P_3) = \tfrac{1}{2}\alpha P_3^2 + \tfrac{1}{4}\left[\gamma - \tfrac{1}{2}s_{ijkl}q_{ij33}q_{kl33}\right]P_3^4 + \tfrac{1}{6}\omega P_3^6 \quad (21)$$

which shows that the fourth-order coefficients are different for the clamped and stress-free boundary conditions, and they are related by

$$\gamma' = \gamma - \tfrac{1}{2}s_{ijkl}q_{ij33}q_{kl33} \quad (22)$$

where γ' is the fourth-order coefficients for the stress-free boundary condition. In general, experimentally determined coefficients correspond to γ', and one has to use Eq. (22) to convert from constant-stress to constant-strain coefficients.

(D) Constant Applied Stress: Under a constant applied stress, the appropriate thermodynamic potential is the elastic Gibbs free energy which can be readily obtained from the Helmholtz-free energy (11) through the Legendre transform,

$$G(\sigma, P_3) = F(\varepsilon_{ij}, P_3) - \sigma_{ij}\varepsilon_{ij} = \tfrac{1}{2}\alpha P_3^2 + \tfrac{1}{4}\gamma P_3^4 + \tfrac{1}{6}\omega P_3^6 + \tfrac{1}{2}c_{ijkl}\varepsilon_{ij}\varepsilon_{kl} - \tfrac{1}{2}q_{ij33}\varepsilon_{ij}P_3^2 - \sigma_{ij}\varepsilon_{ij} \quad (23)$$

Minimizing the free energy (23) with respect to strain,

$$\varepsilon_{ij} = s_{ijkl}\sigma_{kl} + \tfrac{1}{2}s_{ijkl}q_{kl33}P_3^2 \quad (24)$$

Substituting (24) back to the free energy expression (23), we get

$$G(\sigma, P_3) = \tfrac{1}{2}\left[\alpha - s_{ijkl}\sigma_{ij}q_{kl33}\right]P_3^2 + \tfrac{1}{4}\left[\gamma - \tfrac{1}{2}s_{ijkl}q_{ij33}q_{kl33}\right]P_3^4 + \tfrac{1}{6}\omega P_3^6 - \tfrac{1}{2}s_{ijkl}\sigma_{ij}\sigma_{kl}, \quad (25)$$

which shows that the second-order coefficient depends on the applied stress while the fourth-order term is the same as the stress-free boundary condition. With these modified coefficients, one obtains the dependence of the ferroelectric transition temperature and spontaneous polarization on the applied stress.

(E) Mixed Boundary Condition—Thin Film Boundary Condition[2]*:* All the boundary conditions discussed above correspond to either constant strain or constant stress conditions. However, there are examples in which the appropriate boundary condition corresponds to a mixed set of stress and strain boundary conditions. An important example is a single-crystal film constrained by a much thicker substrate. For the sake of discussion, let us consider a simple example of a cubic paraelectric phase transformed to a single tetragonal domain with uniform polarization $(0,0,P_3)$. A constant dilatational plane strain, the biaxial strain, is imposed along the x_1–x_2 directions (Fig. 2) while all the stress components involving the x_3 direction are zero during the transformation, i.e.,

$$\begin{aligned} &\varepsilon_{11} = \varepsilon_{22} = \varepsilon_s \varepsilon_{12} = \varepsilon_{21} = 0, \\ &\sigma_{13} = \sigma_{31} = \sigma_{23} = \sigma_{32} = \sigma_{33} = 0 \end{aligned} \quad (26)$$

where ε_S is the lattice mismatch strain between the film and the substrate. This mixed boundary condition is a good approximation for a (001) oriented cubic single crystal film constrained by a (001) oriented substrate. ε_s may arise from the lattice parameter differences between the film and the substrate for coherent film–substrate interfaces, or from the thermal expansion mismatch between film and substrate for incoherent film–substrate interfaces. For lattice parameter mismatch,

$$\varepsilon_s = \frac{a_s - a_c}{a_c} \quad (27)$$

and for thermal expansion mismatch,

$$\varepsilon_s = \left(T - T_g\right)\left(\alpha_s - \alpha_f\right) \quad (28)$$

where T_g is the film growth temperature, T is the temperature of interest, and α_s and α_f are the linear thermal expansion coefficients of the film and substrate, respectively.

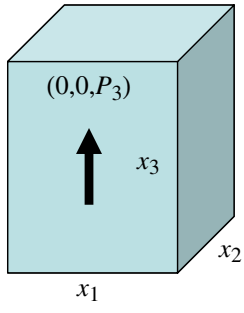

Fig. 2. A schematic illustration of a *c*-domain with polarization along the x_3 direction constraint along the x_1–x_2 directions.

With the above specified mechanical boundary condition for the strain components, the Helmholtz-free energy (11) can be rewritten as

$$F(\varepsilon, P_3) = \tfrac{1}{2}\alpha P_3^2 + \tfrac{1}{4}\gamma P_3^4 + \tfrac{1}{6}\omega P_3^6 - q_{12}\varepsilon_s P_3^2 - \tfrac{1}{2}q_{11}\varepsilon_{33} P_3^2 + (c_{11} + c_{12})\varepsilon_s^2 + 2c_{12}\varepsilon_{33}\varepsilon_s + \tfrac{1}{2}c_{11}\varepsilon_{33}^2 \quad (29)$$

where the electrostrictive coefficients and the elastic constants are expressed in Voigt notation. To satisfy the stress-free boundary condition for the stress components, σ_{13}, σ_{31}, σ_{23}, and σ_{32}, it can immediately be shown that

$$\varepsilon_{13} = \varepsilon_{31} = \varepsilon_{23} = \varepsilon_{32} = 0 \quad (30)$$

The strain component ε_{33} which satisfies the condition, $\sigma_{33} = 0$, is obtained by minimizing the free energy (29) with respect to ε_{33}

$$\varepsilon_{33} = \frac{(q_{11}/2)P_3^2 - 2c_{12}\varepsilon_s}{c_{11}} \quad (31)$$

Therefore, the free energy under the mixed boundary condition is given by

$$F(\varepsilon_s, P_3) = \tfrac{1}{2}\left[\alpha + 2\left(\frac{c_{12}q_{11} - c_{11}q_{12}}{c_{11}}\right)\varepsilon_s\right]P_3^2 + \frac{1}{4}\left[\gamma - \frac{1}{2}\frac{q_{11}^2}{c_{11}}\right]P_3^4 + \tfrac{1}{6}\omega P_3^6 + \left(c_{11} + c_{12} - \frac{2c_{12}^2}{c_{11}}\right)\varepsilon_s^2 \quad (32)$$

in which only the second-order coefficient depends on the mismatch strain, and the Curie–Weiss temperature is given by

$$T_o' = T_o + 2\left(\frac{c_{11}q_{12} - c_{12}q_{11}}{\alpha_1 c_{11}}\right)\varepsilon_s \quad (33)$$

The dependence of Curie–Weiss temperature of a single domain with polarization $(0,0,P_3)$, as a function of substrate constraint for the particular case of $PbTiO_3$ is shown in Fig. 3(a) with the required data taken from Pertsev and colleagues.[2,8]

Similarly, for a single domain with polarization $(P_1,0,0)$ or $(0,P_2,0)$ and the same set of mechanical boundary conditions, the Curie–Weiss temperature as a function of substrate constraint can be obtained from (Fig. 3(b))

$$T_o' = T_o + \left(\frac{c_{11}(q_{11} + q_{12}) - 2c_{12}q_{12}}{\alpha_1 c_{11}}\right)\varepsilon_s \quad (34)$$

One can also establish the relationship between out of plane lattice parameters c, or c/a ratios of the film to the polarization.[9] For example, for a c-domain,

$$\frac{c}{a_{\text{sub}}} = \frac{(c_{11}Q_{11} + 2c_{12}Q_{12})P_3^2 - 2c_{12}\varepsilon_s}{c_{11}(1 + \varepsilon_s)} + 1 \quad (35)$$

or

$$P_3 = \sqrt{\frac{1}{(c_{11}Q_{11} + 2c_{12}Q_{12})}\left[\left(\frac{c}{a_{\text{sub}}} - 1\right)c_{11}(1 + \varepsilon_s) + 2c_{12}\varepsilon_s\right]} \quad (36)$$

For the case of anisotropic in-plane strains, the corresponding equations can also be easily derived.[10,11]

(5) Phase-Field Model of Ferroelectric Domain Structures

In a domain structure, unlike a homogeneous ferroelectric single domain state, the polarization distribution is inhomogeneous, i.e., it depends on the spatial positions. In the phase-field approach, it is the spatial distribution of local polarization $P(x) = (P_1,P_2,P_3)$ that describes a domain structure. Phase-field models have been applied to domain evolution during ferroelectric phase transitions[12–16] and domain switching,[17–26] effect of random defects,[27,28] as well as strain effect on transition temperatures and domain structures in thin films.[29–38]

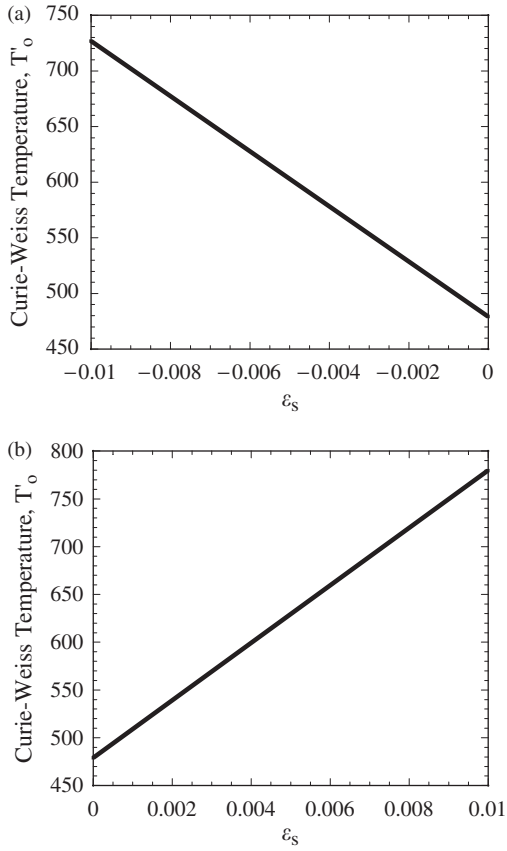

Fig. 3. (a). Curie–Weiss temperature of a single domain with polarization $(0,0,P_3)$ as a function of constraint for (001) $PbTiO_3$ single crystal films on a (001) oriented cubic substrate. (b). Curie–Weiss temperature of a single domain with polarization $(P_1,0,0)$ or $(0,P_2,0)$ as a function of constraint for (001) $PbTiO_3$ single crystal films on a (001) oriented cubic substrate.

The total-free energy of an inhomogeneous domain structure is given by Ginzburg–Landau free energy functional:

$$F = \int_V [f_{\text{bulk}}(P_i) + f_{\text{grad}}(\partial P_i/\partial x_j) + f_{\text{elast}}(P_i, \varepsilon_{ij}) + f_{\text{elec}}(P_i, E_i)]\mathrm{d}^3x \quad (37)$$

in which f_{bulk} is the bulk free-energy density (Eqs. (4) or (5)) and f_{grad} is the gradient energy that is only nonzero around domain walls and other interfaces where the polarization is inhomogeneous,

$$f_{\text{wall}} = \tfrac{1}{2}G_{ijkl}P_{i,j}P_{k,l} \quad (38)$$

where $P_{i,j} = \partial P_i/\partial x_j$ and G_{ijkl} are the gradient energy coefficients.

To obtain the elastic strain energy density, f_{elast}, the mechanical equilibrium equation has to be solved for a given domain structure. For a bulk single crystal with periodic boundary conditions, one can use the Khachaturyan's elasticity theory,[39]

$$\int_V f_{\text{elast}}\mathrm{d}^3x = \frac{V}{2}c_{ijkl}\bar{\varepsilon}_{ij}\bar{\varepsilon}_{kl} - c_{ijkl}\bar{\varepsilon}_{ij}\int_V \varepsilon^o_{kl}(x)\mathrm{d}^3x + \tfrac{1}{2}c_{ijkl}\int_V \varepsilon^o_{ij}(x)\varepsilon^o_{kl}(x)\mathrm{d}^3x - \tfrac{1}{2}\int \frac{\mathrm{d}^3g}{(2\pi)^3} n_i \boldsymbol{\sigma}^o_{ij}(\boldsymbol{g})\Omega_{jk}\left[\sigma^o_{kl}(\boldsymbol{g})\right]^* n_l \quad (39)$$

Where

$$\varepsilon^o_{ij}(\boldsymbol{x}) = Q_{ijkl}P_k(\boldsymbol{x})P_l(\boldsymbol{x}) \quad (40)$$

$$\sigma^o_{ij}(x) = c_{ijkl}\varepsilon^o_{kl}(x) \quad (41)$$

$$\sigma^o_{ij}(\boldsymbol{g}) = \int_V \sigma^o_{ij}(x)e^{-i\boldsymbol{g}\bullet x}\mathrm{d}^3x$$
$$\Omega^{-1}_{ik} = c_{ijkl}n_j n_l \quad (42)$$

$\left[\boldsymbol{\sigma}^o_{kl}(\boldsymbol{g})\right]^*$ means the complex conjugate of $\boldsymbol{\sigma}^o_{ij}(\boldsymbol{g})$.

It can be seen that the elastic energy is a function of elastic properties, transformation crystallography, and the domain structure. The homogeneous strain, $\bar{\varepsilon}_{ij}$, is to be determined from the boundary conditions.[39,40] Expression (39) can be used to calculate the elastic energy of an arbitrary domain structure described by the spontaneous polarization distribution, $\boldsymbol{P}(\mathbf{x})$, under the assumption of homogeneous elastic modulus. For the case of elastically inhomogeneous case, a perturbation method may be used.[41–43]

For thin films, the mechanical boundary conditions become more complicated. As shown in Fig. 4, the top surface is stress-free and the bottom surface is constrained by the substrate. As it has been shown previously,[29,30] the solution to the mechanical equilibrium equations for a film–substrate system can be obtained by combining Khachaturyan's mesoscopic elasticity theory[39,44] and the Stroh formalism of anisotropic elasticity.[45]

Similarly, the electrical energy density, f_{elec}, can be obtained by solving the electrostatic equation. For the simple case that the depolarization field is compensated and the external field is uniform, we have

$$\int_V f_{\text{elec}}\mathrm{d}^3V = \tfrac{1}{2}\int \frac{\left|n_i P^o_i(\boldsymbol{g})\right|^2}{n_j\kappa_{jk}n_k}\frac{\mathrm{d}^3g}{(2\pi)^3} - \left(E^{\text{ex}}_i\bar{P}_i\right)V \quad (43)$$

where $P^o_k(g) = \int_V P^o_k(x)e^{-i\boldsymbol{g}\bullet x}\mathrm{d}^3x$, κ_{jk} is the dielectric constant tensor, E^{ex} is the homogeneous external electric field. In Eq. (43), the reciprocal space origin, $\boldsymbol{g} = 0$, is excluded in the integration. Equation shows the dependence of electrostatic energy on dielectric constants, the domain structure, and the external applied field. The electrostatic solutions for different electrical boundary conditions for a film/substrate system can be obtained using the same strategy as the elastic solution for thin films.[46]

With all the important energetic contributions to the total-free energy, the temporal evolution of the polarization vector field, and thus the domain structure, is then described by the time-dependent Ginzburg-Landau (TDGL) equations,

$$\frac{\partial P_i(x,t)}{\partial t} = -L\frac{\delta F}{\delta P_i(x,t)} \quad (44)$$

where L is the kinetic coefficient related to the domain-wall mobility. Eq. (44) can be quite efficiently solved using the semi-implicit Fourier-spectral method.[47]

II. Examples

(1) $PbTiO_3$ Thin Films[29,30]

$PbTiO_3$ is a prototype perovskite ferroelectric which undergoes a cubic to tetragonal ferroelectric phase transition when the paraelectric phase is cooled below the Curie temperature at around 470°C. For a (001)-oriented thin film on a (001)-oriented cubic substrate, the oriented variants are conventionally labeled as a_1, a_2, and c, respectively. If the coordinate system (x_1, x_2, x_3) is a rectangular coordinate system originated at the film–substrate interface with x_3 normal to the film, the polarization vectors are $\boldsymbol{P} = (P_1,0,0)$ for a_1-domain, $\boldsymbol{P} = (0,P_2,0)$ for a_2-domain, and $\boldsymbol{P} = (0,0,P_3)$ for c-domain, respectively (Fig. 4).

Figure 5 shows the stability regions of various domain structures at different temperatures and strains, i.e., the domain stability map, for (001)-oriented $PbTiO_3$ films obtained by phase-field simulations. All the data points shown in Fig. 5 were obtained by starting from an initial paraelectric state with small random perturbations. The data points simply represent the type of domain structures existed at the end of a sufficiently long simulation. Because of the numerical nature of the calculations, the lines which separate the stability of different types of domain structures cannot be determined exactly, i.e., they are approximate. As shown in Fig. 5, for a given temperature, the equilibrium domain structures are a single c-domain state, a $c/a_1/a_2$ three-domain state, and a a_1/a_2 two-domain state, respectively, as the substrate constraint changes from compressive to tensile.

Examples of three-types of domain structures are shown in Fig. 6 in which an iso-surface of a given polarization component is shown. While Fig. 6(a) is a c-domain state with 180°C domain walls along the out-of-plane direction, only the a_1- and a_2-

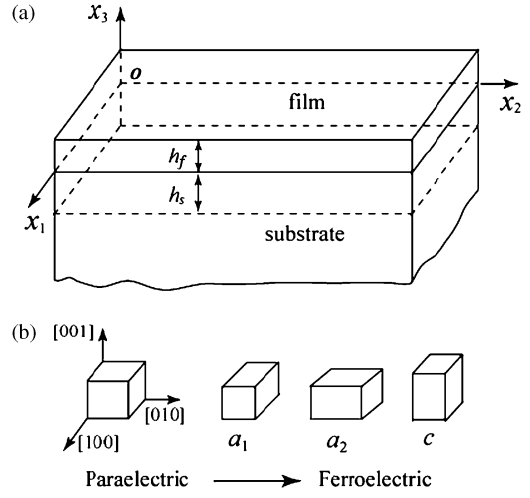

Fig. 4. Schematic illustrations, (a) a thin film coherently constrained by a substrate, and (b) schematic illustration of cubic paraelectric phase and the three ferroelectric tetragonal variants. (from[29,30])

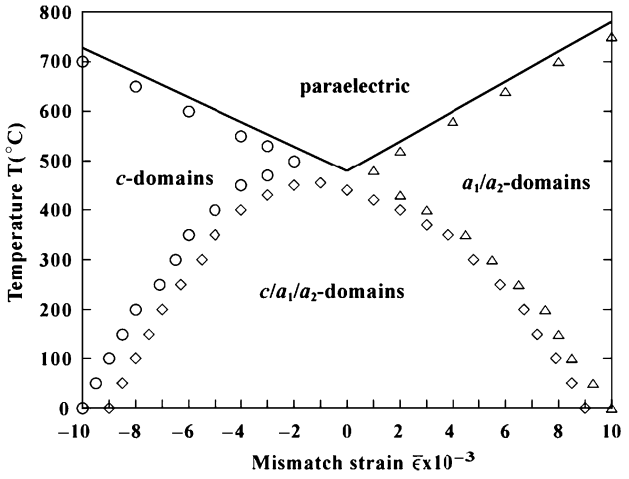

Fig. 5. The domain stability map of a film: the equilibrium phases or domain structures as a function of temperature and substrate constraint, obtained from phase-field simulations assuming coherent interface between the film and the substrate.[29,30]

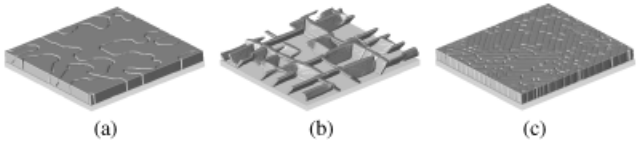

Fig. 6. Domain structures at 25°C: (a) *c*-domains with 180° domain walls ($\varepsilon_s = -0.012$); (b) $c/a_1/a_2$ domain structure with 24% of *a*-domains ($\varepsilon_s = -0.002$); (c) a_1/a_2 domain structure ($\varepsilon_s = 0.012$) (from[29,30]).

domains are shown in Fig. 6(b) and (c). The domain walls between *c* and *a* are approximately 45° from the film/substrate interface while the a_1/a_2 twin walls are vertical along the out-of-plane directions. It is noted that the lattice symmetry of a_1/a_2 domains under a substrate constraint is, strictly speaking, orthorhombic rather than tetragonal.

It should be pointed out that while phase-field simulations do not assume the domain wall orientations as *a priori*, qualitatively different versions of strain diagrams have been obtained from thermodynamic calculations for the (001)-oriented $PbTiO_3$ films as a result of different assumptions.[2,5,6] For example, the a_1/a_2 domain configurations with vertical domain walls under a large tensile constraint were predicted in phase-field simulations, whereas an incorrect domain configuration consisting of distorted orthorhombic phases was obtained by thermodynamic calculations assuming a single domain or a_1/a_2 domain walls oriented 45° from the film/substrate interface under a similar tensile mismatch.[5] Changing the assumption of domain wall orientation from being 45° to vertical from the film/substrate interface[6] in the thermodynamic analysis leads to the same conclusion that a_1/a_2 domain configuration is the stable state under a tensile constraint as in the phase-field simulation. Quantitative difference between thermodynamic calculations and phase-field simulations may also result from the assumptions on the number of types of domains that may coexist in a domain structures. For example, the phase-field simulation results show that a_1- and a_2-domains always coexist, whereas in thermodynamic analyses, simplified domain structures, either $c/a_1/c/a_1$ or $c/a_2/c/a_2$, were assumed, which can not completely accommodate the biaxial constraint along the x_1 and x_2 axes.[5,6] As a result, although the qualitatively correct domain stability map can be obtained with correct domain wall orientations, the border lines separating the stability regions of different domain states can be significantly shifted due to the assumption of two-dimensional (2D) domain structures. Furthermore, domain walls of different orientations can also coexist in a given domain structure. For example, in a $c/a_1/a_2$ domain state, when the volume fraction of *c*-domains is small, there are a significant number of domains walls between a_1- and a_2-domains which are perpendicular to the film–substrate interface while the domains between c and a domains are approximately 45° from the film/substrate interface. Therefore, it is inaccurate to assume that all domain walls within a $c/a/c/a$ domain structures are 45° from the film–substrate interface. Finally, phase-field simulations demonstrate that the domain wall orientations of *c*- and *a*-domains are not exactly along the directions 45° from the film–substrate interface which was typically assumed in thermodynamic analysis.

(2) $BaTiO_3$ Thin Films[35,48]

The phase transitions in $BaTiO_3$ are more complicated than $PbTiO_3$. It involves a number of phase transitions in the bulk:

$$\text{Cubic} \xrightarrow{125^\circ\text{C}} \text{Teragonal} \xrightarrow{8^\circ\text{C}} \text{Orthorhombic} \xrightarrow{-71^\circ\text{C}} \text{Rhombohedral}$$

Each of these transitions involves not only a change in spontaneous polarization direction but also lattice parameters, and hence it is expected that all the transition temperatures will be shifted as a result of substrate strain in a $BaTiO_3$ film. The

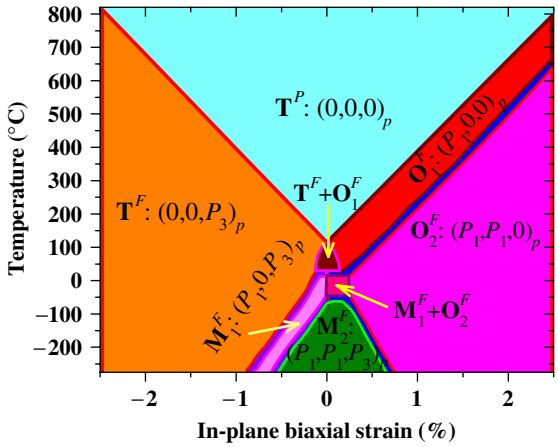

Fig. 7. Phase diagram of $BaTiO_3$ films as a function of temperature and substrate constraint strain. T^P—tetragonal paraelectric, T^F—tetragonal ferroelectric, O^F—orthorhombic ferroelectric, and M^F—monoclinic ferroelectric (From Li *et al.*[35,48]).

amount of shifts will depend on the film orientation, the degree of coherency between film and substrate, temperature, and the strain magnitude, and anisotropy. With multiple phase transitions and many possible domain wall orientations, it is very difficult to construct strain diagrams using thermodynamic calculations. For the particular case of (001)-oriented $BaTiO_3$ film under a symmetrical biaxial constraint, the phase transition temperatures and domain stabilities as a function of strain have been obtained using phase-field simulations (Fig. 7).[35] As in the $PbTiO_3$ case, all the simulations started from a homogeneous paraelectric state with a small random noise of uniform distribution. The various ferroelectric phases were labeled by lattice symmetries, determined by the non-zero components of local polarization. At high temperatures, as expected, the paraelectric phase is the stable state which has a tetragonal symmetry (T^p) due to the biaxial strain. For the same reason, the tetragonal *a*-domains and the rhombohedral phase were marked as orthorhombic (O_1^F)and monoclinic (M_1^F), respectively in Fig. 7.

Examples of domain structures from the simulations are shown Fig. 8.[35,48] Under sufficiently large compressive strains ($> \sim -0.8\%$), there is only one ferroelectric transition, and the rest disappears. The ferroelectric phase is of tetragonal symmetry (T^P) with polarization directions orthogonal to the film/substrate interface. Figure 8(a) is a typical domain structure under large compressive strains, in which there are two types of *c*-domains (c^+ and c^-) separated by 180° domain walls. On the tensile side, there are only two ferroelectric phase transitions for strain values greater than $\sim +0.6\%$. The polarization directions for the two ferroelectric phases are parallel to the film/substrate interface, either along [100] (O_1^F)) or [110] (O_2^F) direction, depending on temperature and the magnitude of strain. The corresponding domain structures are similar to either the a_1/a_2 twins as shown in Fig. 8(c), or the orthorhombic twins of Fig. 8(f), or the mixture of them shown in Fig. 8(g). Under relatively smaller strains, the ferroelectric phase transitions and domain structures of various ferroelectric phases are similar to bulk single crystals. At room temperature, the domain structures vary from pure *c*-domains to $c/a_1/a_2$ then to a_1/a_2 twins, a mixture of a_1/a_2 and O_1/O_2 twins, and O_1/O_2 twins when substrate constraint changes from compressive to tensile. It is noted that there are also other narrow regions in which more than two or more ferroelectric phases coexist.

(3) $PbZr_xTi_{1-x}O_3$ (PZT) Thin Films[31,33,34]

For PZT thin films, the strain-temperature diagram is composition dependent. Both thermodynamic theories and phase-field simulations have been used to study the phase stability, domain structures and properties at different strains and compositions.

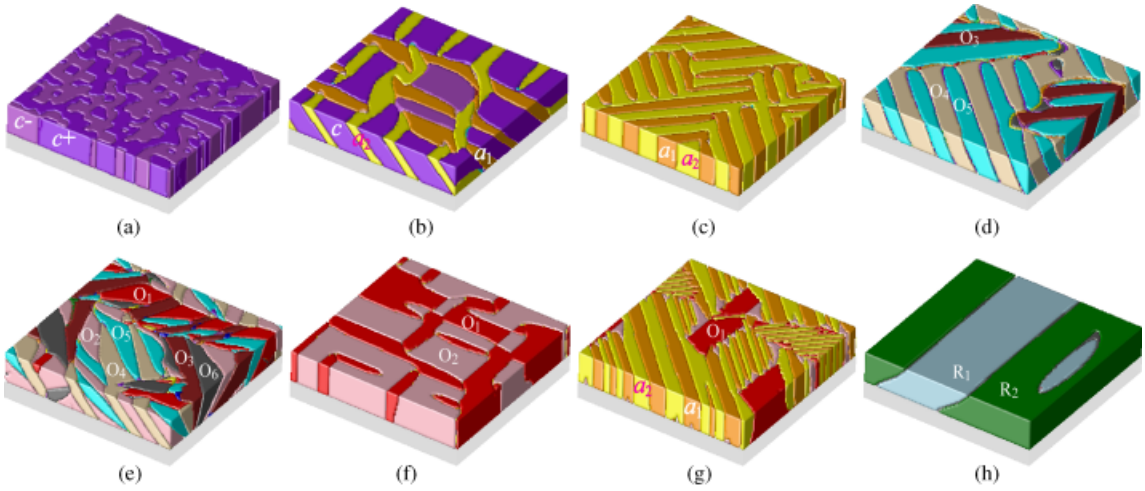

Fig. 8. Representative domain morphologies in $BaTiO_3$ films within different domain stability fields. Domain definitions: a_1: $(P_1,0,0)$; a_2: $(0,P_1,0)$; c^+: $(0,0,+P_3)$; c^-: $(0,0,-P_3)$; R_1: $(-P_1,-P_1,P_3)$; R_2: $(P_1,-P_1,P_3)$; O_1: $(P_1,P_1,0)$; O_2: $(P_1,-P_1,0)$; O_3: $(P_1,0,P_3)$; O_4: $(P_1,0,-P_3)$; O_5: $(0, P_1,P_3)$; O_6: $(0, P_1,-P_3)$. (a) T^F at $T=25°C$ and $e_0=-1.0\%$; (b) $T^F+O_1^F$ at $T=75°C$ and $e_0=0.0$; (c) O_1^F at $T=50°C$ and $e_0=0.2\%$; (d) $T^F+O_1^F$ at $T=-25°C$ and $e_0=-0.05\%$; (e) O_2^F at $T=-25°C$ and $e_0=0.1\%$; (f) O_2^Fat $T=25°C$ and $e_0=1.0\%$; (g) $O_1^F+O_2^F$ at $T=25°C$ and $e_0=0.25\%$; (h) M_2^F at $T=-00°C$ and $e_0=0.1\%$. (From Li *et al.*[35,48]).

It is shown that for the case of $PbTiO_3$-rich PZT (e.g., $PbZr_{0.2}Ti_{0.8}O_3$) thin films, the strain diagram is similar to pure $PbTiO_3$ thin films. Near the morphotropic boundary condition, a temperature-strain diagram was constructed using phase-field simulations for a (001)-oriented PZT epitaxial single crystal thin film on an (001)-oriented cubic substrate.[33] According to the strain diagram, a mixture of distorted rhombohedral, orthorhombic, and tetragonal phases coexist near strain equal to zero. This result is in contrast to a single distorted rhombohedral phase predicted from thermodynamic calculations assuming a single-domain state under a similar strain. Under a large tensile strain, a distorted tetragonal phase with a_1/a_2 twin structures is the stable state, while the thermodynamics predicted an orthorhombic phase.

The phase diagrams of a PZT film under a number of different strains were also calculated by thermodynamics (Fig. 9(a)) and phase-field simulations (Fig. 9(b)).[31] As in $PbTiO_3$ and $BaTiO_3$, substrate strain always increases the ferroelectric transition temperature, and the maximum effect is around the morphotropic boundary composition. Both in the thermodynamic calculations and phase-field simulations, an orthorhombic phase that does not exist in the bulk becomes stable under a tensile constraint. However, the stability region for the (distorted) tetragonal phase is much wider than that obtained from the thermodynamic calculations assuming a single domain.

The ferroelectric domain morphologies and domain wall orientations of the rhombohedral, orthorhombic, and tetragonal domains have also been modeled using phase-field simulations as a function of composition, temperature, substrate constraint, and the electrostatic boundary condition.[34]

(4) Phase Transitions of $(BaTiO_3)_n/(SrTiO_3)_m$ Superlattices[37,49]

The phase transitions and domain structures of $(BaTiO_3)_n/(SrTiO_3)_m$ superlattices were recently studied by the phase-field method, where n and m represent the number of ferroelectric (001) oriented $BaTiO_3$ perovskite unit cells and nonferroelectric (001) oriented $SrTiO_3$ unit cells, respectively along the growth direction.

Figure 10(a) shows a schematic superlattice consisting of periodically alternating (001) $SrTiO_3$ and (001) $BaTiO_3$ layers on a (001) $SrTiO_3$ substrate. The top surface and the film/substrate interface are assumed to be both charge compensated.

Figure 11 shows the plots of ferroelectric transition temperatures at different $BaTiO_3$ and $SrTiO_3$ layer thicknesses within the

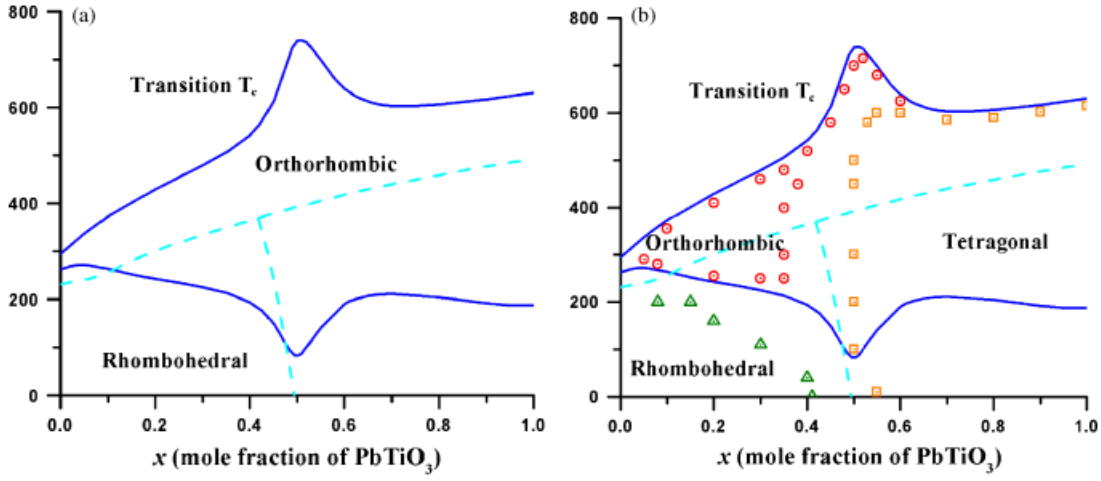

Fig. 9. (a). Phase diagram of PZT film under a biaxial compressive strain of 0.5% calculated from thermodynamics assuming a single-domain state. The dashed line is the bulk phase-diagram under the stress-free condition. (b) The symbols represent the ferroelectric domain states obtained phase-field simulations: squares—tetragonal circles—orthorhombic, and triangles—distorted rhombohedral (from Li *et al.*[31]).

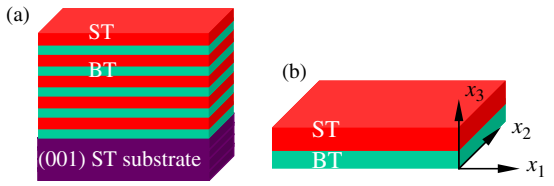

Fig. 10. Schematic structure of an epitaxial and commensurate $(BaTiO_3)_n/(SrTiO_3)_m$ superlattice on a substrate (a) and the simulation cell (b). (from Tenne and colleagues[37,49]).

superlattice (n and m) predicted from phase-field simulations, UV Raman and variable-temperature X-ray diffraction (VTXRD) measurements of MBE-grown samples.[50] 3D indicates phase-field simulations which were performed allowing 3D inhomogeneity in polarization ($\mathbf{P} = \mathbf{P}(x_1,x_2,x_3)$) and thus 3D domain structures while 1D represents simulations of only allowing 1D inhomogeneity in polarization ($\mathbf{P} = \mathbf{P}(x_3)$). It is shown that the transition temperatures predicted from phase-field simulations allowing 3D polarization inhomogeneity show excellent agreement with experimentally measured values.

It should be pointed out that for the $(BaTiO_3)_n/(SrTiO_3)_m$ superlattices which are commensurate the (001) $SrTiO_3$ substrate, the $SrTiO_3$ layers in the superlattices are not ferroelectric; they only possess polarization induced by the neighboring $BaTiO_3$. On the other hand, $(BaTiO_3)_n/(SrTiO_3)_m$ superlattices which are either partially or fully relaxed, the $SrTiO_3$ layers are ferroelectric as a result of the in-plane biaxial tensile strain from the adjacent $BaTiO_3$ layers. In this case, it has been shown that the ferroelectric $SrTiO_3$ layers are of orthorhombic symmetry.[4,36,51–53]

III. Summary Remarks

Applications of phase-field method to phase transitions and domain structures in ferroelectric thin films are briefly reviewed. The focus was on the strain effect on the transition temperatures and stability of competing ferroelectric phases and domain structures. It is shown that without any *a priori* assumptions on the type of domain structures that might form under a given substrate constraint and temperature, the phase-field method is able to predict not only the effect of substrate constraint on phase transition temperatures and the volume fractions of domains, but also the detailed domain structures and their temporal evolution during a ferroelectric transition of both single-phase films and superlattices.

In addition to $PbTiO_3$, $BaTiO_3$, PZT, and $BaTiO_3/SrTiO_3$ superlattices briefly discussed above, the phase-field method has been applied to predicting domain structures of $SrBi_2Nb_2O_9$ epitaxial thin films,[54] interactions between ferroelastic and ferroelectric domains in strained $SrTiO_3$,[36,53] polarization,[55] domain structures[56] and domain switching[57] of multiferroic $BiFeO_3$ films, as well as morphologies[58] and magnetoelectric coupling[59] of ferroelectric and ferromagnetic nanocomposites.

Using the micromechanics concept of eigenstrains, it is possible to introduce any arbitrary distribution of dislocations in a phase-field model, and it has been applied to the domain nucleation and spatial distribution. There have also been attempts to study the various factors that influence the coercive field in bulk single crystals, ceramics, and thin films, including existing domain walls,[26,60,61] twin wall width,[25,62] grain boundaries,[63–65] dislocations[66–68] as well as strain.[69]

There have been a number of other recent developments in the applications of phase-field to ferroelectrics. Examples include the coupling between charge density and domain structures,[70] domain structures of ferroelectric islands,[71] switching and piezoelectricity[72] of ferroelectric islands, and effect of fracture on domain switching.[73,74]

The main limitation associated with the phase-field method is the fact that it requires input information for thermodynamic and kinetic parameters. While the thermodynamics of a number of well-known ferroelectrics are known, the information about domain wall energy and domain wall mobility is much scarcer. For example, quantifying the domain wall kinetics directly from the phase-field method is possible only if the intrinsic domain wall mobility is available. Furthermore, phase-field method is based on the continuum phenomenological description, so the detailed atomistic mechanisms associated with domain evolution are not accessible. A future direction along this line is to link first-principles calculations for structural properties and the phase-field method of domain structure evolution.

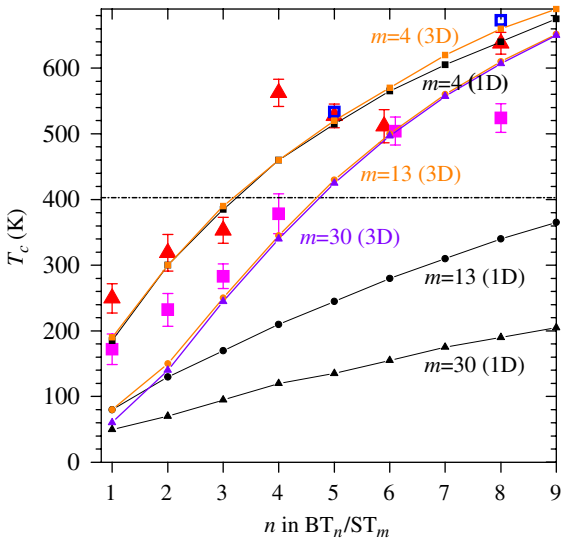

Fig. 11. Ferroelectric transition temperatures of $(BaTiO_3)_n/(SrTiO_3)_m$ superlattices on (001) a $SrTiO_3$ substrate. Blue and black triangles represent the predictions from the phase-field calculations allowing three dimensional and one dimensional inhomogeneity in polarization, respectively. Pink squares ($m = 13$) and red triangles ($m = 4$) were measured by ultra-violet Raman spectroscopy, and the open squares were determined from variable temperature X-ray diffraction measurements of lattice parameters ($m = 4$). (from Tenne and colleagues[37,49]).

Acknowledgments

He also would like to express his gratitude for the hard work of his postdoctors and students, Dr. Y. L. Li, S. Choudhury, Dr. S. Y. Hu, and J. X. Zhang. In particular, Y. L. Li has been instrumental in developing phase-field models of domain structures in ferroelectric thin films. He would like to thank many of his collaborators for their ideas, discussions, suggestions and encouragement, including D. G. Schlom, X. X. Xi, V. Gopalan, R. Ramesh, C. B. Eom, S. Kalinin, Q. X. Jia, T. Lookman, A. Saxena, S. Streiffer, S. Trolier-McKinstry, J. Levy, K. Rabe, and their students and postdoctors.

References

[1]D. G. Schlom, L. Q. Chen, C. B. Eom, K. M. Rabe, S. K. Streiffer, and J. M. Triscone, "Strain Tuning of Ferroelectric Thin Films," *Ann. Rev. Mater. Res.*, **37**, 589–626 (2007).

[2]N. A. Pertsev, A. G. Zembilgotov, and A. K. Tagantsev, "Effect of Mechanical Boundary Conditions on Phase Diagrams of Epitaxial Ferroelectric Thin Films," *Phys. Rev. Lett.*, **80** [9] 1988–91 (1998).

[3]K. J. Choi, M. Biegalski, Y. L. Li, A. Sharan, J. Schubert, R. Uecker, P. Reiche, Y. B. Chen, X. Q. Pan, V. Gopalan, L. Q. Chen, D. G. Schlom, and C. B. Eom, "Enhancement of Ferroelectricity in Strained $BaTiO_3$ Thin Films," *Science*, **306** [5698] 1005–9 (2004).

[4]J. H. Haeni, P. Irvin, W. Chang, R. Uecker, P. Reiche, Y. L. Li, S. Choudhury, W. Tian, M. E. Hawley, B. Craigo, A. K. Tagantsev, X. Q. Pan, S. K. Streiffer, L. Q. Chen, S. W. Kirchoefer, J. Levy, and D. G. Schlom, "Room-Temperature Ferroelectricity in Strained $SrTiO_3$," *Nature*, **430** [7001] 758–61 (2004).

[5]N. A. Pertsev and V. G. Koukhar, "Polarization Instability in Polydomain Ferroelectric Epitaxial Thin Films and the Formation of Heterophase Structures," *Phys. Rev. Lett.*, **84** [16] 3722–5 (2000).

[6]V. G. Koukhar, N. A. Pertsev, and R. Waser, "Thermodynamic Theory of Epitaxial Ferroelectric Thin Films with Dense Domain Structures," *Phys. Rev. B*, **6421**, -214103 (2001).

[7]A. Devonshire, "Phenomenological Theory of High Permittivity in Fine-Grained Barium Titanate," *Philos. Mag.*, **40**, 1040 (1949).

[8]M. J. Haun, E. Furman, S. J. Jang, H. A. Mckinstry, and L. E. Cross, "Thermodynamic Theory of Pbtio3," *J. Appl. Phys*., **62** [8] 3331–8 (1987).
[9]D. D. Fong, C. Cionca, Y. Yacoby, G. B. Stephenson, J. A. Eastman, P. H. Fuoss, S. K. Streiffer, C. Thompson, R. Clarke, R. Pindak, and E. A. Stern, "Direct Structural Determination in Ultrathin Ferroelectric Films by Analysis of Synchrotron X-Ray Scattering Measurements," *Phy. Rev. B*, **71**, 144112 (2005).
[10]J. Wang and T. Y. Zhang, "Effects of Nonequally Biaxial Misfit Strains on the Phase Diagram and Dielectric Properties of Epitaxial Ferroelectric Thin Films," *Appl. Phys. Lett*., **86**, 192905 (2005).
[11]A. G. Zembilgotov, N. A. Pertsev, U. Bottger, and R. Waser, "Effect of Anisotropic in-Plane Strains on Phase States and Dielectric Properties of Epitaxial Ferroelectric Thin Films," *Appl. Phys. Lett*., **86**, 052903 (2005).
[12]S. Nambu and D. A. Sagala, "Domain Formation and Elastic Long-Range Interaction in Ferroelectric Perovskites," *Phys. Rev. B*, **50** [9] 5838–47 (1994).
[13]W. Yang and L. Q. Chen, "Computer-Simulation of the Dynamics of 180-Degrees Ferroelectric Domains," *J. Am. Ceram. Soc*., **78** [9] 2554–6 (1995).
[14]H. L. Hu and L. Q. Chen, "Computer Simulation of 90 Degrees Ferroelectric Domain Formation in Two-Dimensions," *Mater. Sci. Eng.-Struct. Mater. Properties Microstruct. Proc*., **238** [1] 182–91 (1997).
[15]H. L. Hu and L. Q. Chen, "Three-Dimensional Computer Simulation of Ferroelectric Domain Formation," *J. Am. Ceram. Soc*., **81** [3] 492–500 (1998).
[16]A. Kuroda, K. Ozawa, Y. Uesu, and Y. Yamada, "Simulation Study of Zigzag Domain Boundary Formation in Ferroelectric—Ferroelastics using the TDGL Equation," *Ferroelectrics*, **219** [1–4] 851–60 (1998).
[17]R. Ahluwalia and W. W. Cao, "Effect of Surface Induced Nucleation of Ferroelastic Domains on Polarization Switching in Constrained Ferroelectrics," *J. Appl. Phys*., **93** [1] 537–44 (2003).
[18]J. Wang, S. Q. Shi, L. Q. Chen, Y. L. Li, and T. Y. Zhang, "Phase Field Simulations of Ferroelectric/Ferroelastic Polarization Switching," *Acta Materialia*, **52** [3] 749–64 (2004).
[19]R. Ahluwalia, T. Lookman, A. Saxena, and W. Cao, "Piezoelectric Response of Engineered Domains in Ferroelectrics," *Appl. Phys. Lett*., **84** [18] 3450–2 (2004).
[20]R. Ahluwalia, T. Lookman, A. Saxena, and W. W. Cao, "Domain-Size Dependence of Piezoelectric Properties of Ferroelectrics," *Phys. Rev. B*, **72**, 014112 (2005).
[21]W. Zhang and K. Bhattacharya, "A Computational Model of Ferroelectric Domains. Part I: Model Formulation and Domain Switching," *Acta Materialia*, **53** [1] 185–98 (2005).
[22]A. K. Soh, Y. C. Song, and Y. Ni, "Phase Field Simulations of Hysteresis and Butterfly Loops in Ferroelectrics Subjected to Electro-Mechanical Coupled Loading," *J. Am. Ceram. Soc*., **89** [2] 652–61 (2006).
[23]Y. Su and C. M. Landis, "Continuum Thermodynamics of Ferroelectric domain Evolution: Theory, Finite Element Implementation, and Application to Domain Wall Pinning," *J. Mech. Phys. Solids*, **55** [2] 280–305 (2007).
[24]W. F. Rao and Y. U. Wang, "Bridging Domain Mechanism for Phase Coexistence in Morphotropic Phase Boundary Ferroelectrics," *Appl. Phys. Lett*., **90**, 182906 (2007).
[25]W. F. Rao and Y. U. Wang, "Domain Wall Broadening Mechanism for Domain Size Effect of Enhanced Piezoelectricity in Crystallographically Engineered Ferroelectric Single Crystals," *Appl. Phys. Lett*., **90** [4] (2007).
[26]S. Choudhury, L. Q. Chen, and Y. L. Li, "Correlation Between Number of Ferroelectric Variants and Coercive Field of Lead Ziconate Titanate Single Crystals," *Appl. Phys. Lett*., **91** [3] (2007).
[27]S. Semenovskaya and A. G. Khachaturyan, "Development of Ferroelectric Mixed States in a Random Field of Static Defects," *J. Appl. Phys*., **83** [10] 5125–36 (1998).
[28]S. Semenovskaya and A. G. Khachaturyan, "Ferroelectric Transition in a Random Field: Possible Relation to Relaxor Ferroelectrics," *Ferroelectrics*, **206** [1–4] 157–80 (1998).
[29]Y. L. Li, S. Y. Hu, Z. K. Liu, and L. Q. Chen, "Phase-Field Model of Domain Structures in Ferroelectric Thin Films," *Appl. Phys. Lett*., **78** [24] 3878–80 (2001).
[30]Y. L. Li, S. Y. Hu, Z. K. Liu, and L. Q. Chen, "Effect of Substrate Constraint on the Stability and Evolution of Ferroelectric Domain Structures in Thin Films," *Acta Materialia*, **50** [2] 395–411 (2002).
[31]Y. L. Li, S. Choudhury, Z. K. Liu, and L. Q. Chen, "Effect of External Mechanical Constraints on the Phase Diagram of Epitaxial $PbZr_{1-x}Ti_xO_3$ Thin Films—Thermodynamic Calculations and Phase-Field Simulations," *Appl. Phys. Lett*., **83** [8] 1608–10 (2003).
[32]D. A. Tenne, X. X. Xi, Y. L. Li, L. Q. Chen, A. Soukiassian, M. H. Zhu, A. R. James, J. Lettieri, D. G. Schlom, W. Tian, and X. Q. Pan, "Absence of Low-Temperature Phase Transitions in Epitaxial $BaTiO_3$ Thin Films," *Phys. Rev. B*, **69**, 174101 (2004).
[33]S. Choudhury, Y. L. Li, and L. Q. Chen, "A Phase Diagram for Epitaxial $PbZr_{1-x}Ti_xO_3$ Thin Films at the Bulk Morphotropic Boundary Composition," *J. Am. Ceram. Soc*., **88** [6] 1669–72 (2005).
[34]Y. L. Li, S. Y. Hu, and L. Q. Chen, "Ferroelectric Domain Morphologies of (001)$PbZr_{1-x}Ti_xO_3$ Epitaxial Thin Films," *J. Appl. Phys*., **97**, 034112 (2005).
[35]Y. L. Li and L. Q. Chen, "Temperature-Strain Phase Diagram for $BaTiO_3$ Thin Films," *Appl. Phys. Lett*., **88**, 072905 (2006).
[36]Y. L. Li, S. Choudhury, J. H. Haeni, M. Biegalski, A. Vasudevarao, A. Sharan, H. Z. Ma, J. Levy, V. Gopalan, S. Trolier-Mckinstry, D. G. Schlom, Q. X. Jia, and L. Q. Chen, "Phase Transitions and Domain Structures in Strained Pseudocubic (100) $SrTiO_3$ Thin Films," *Phys. Rev. B*, **73**, 184112 (2006).
[37]D. A. Tenne, A. Bruchhausen, N. D. Lanzillotti-Kimura, A. Fainstein, R. S. Katiyar, A. Cantarero, A. Soukiassian, V. Vaithyanathan, J. H. Haeni, W. Tian, D. G. Schlom, K. J. Choi, D. M. Kim, C. B. Eom, H. P. Sun, X. Q. Pan, Y. L. Li, L. Q. Chen, Q. X. Jia, S. M. Nakhmanson, K. M. Rabe, and X. X. Xi, "Probing Nanoscale Ferroelectricity by Ultraviolet Raman Spectroscopy," *Science*, **313** [5793] 1614–6 (2006).
[38]V. Vaithyanathan, J. Lettieri, W. Tian, A. Sharan, A. Vasudevarao, Y. L. Li, A. Kochhar, H. Ma, J. Levy, P. Zschack, J. C. Woicik, L. Q. Chen, V. Gopalan, and D. G. Schlom, "*c*-axis Oriented Epitaxial $BaTiO_3$ Films on (001) Si," *J. Appl. Phys*., **100**, 024108 (2006).
[39]A. G. Khachaturyan, *Theory of Structural Transformations in Solids*. John Wiley & Sons, New York, 1983.
[40]D. Y. Li and L. Q. Chen, "Morphological Evolution of Coherent Multivariant $Ti_{11}Ni_{14}$ Precipitates in Ti–Ni Alloys Under an Applied Stress—A Computer Simulation Study," *Acta Materialia*, **46** [2] 639–49 (1998).
[41]A. G. Khachaturyan, S. Semenovskaya, and T. Tsakalakos, "Elastic Strain Energy of Inhomogeneous Solids," *Phys. Rev. B*, **52**, 1–11 (1995).
[42]S. Y. Hu and L. Q. Chen, "A Phase-Field Model for Evolving Microstructures with Strong Elastic Inhomogeneity," *Acta Materialia*, **49** [11] 1879–90 (2001).
[43]P. Yu, S. Y. Hu, L. Q. Chen, and Q. Du, "An Iterative-Perturbation Scheme for Treating Inhomogeneous Elasticity in Phase-Field Models," *J. Computational Phys*., **208** [1] 34–50 (2005).
[44]A. G. Khachaturyan and G. A. Shatalov, "Theory of Macroscopic Periodicity for A Phase Transition in Solid State," *Sov. Phys. JETP (Engl. Transl.)*, **29**, 557 (1969).
[45]A. N. Stroh, "Steady State Problems in Anisotropic Elasticity," *J. Math. Phys*., **41**, 77 (1962).
[46]Y. L. Li, S. Y. Hu, Z. K. Liu, and L. Q. Chen, "Effect of Electrical Boundary Conditions on Ferroelectric Domain Structures in Thin Films," *Appl. Phys. Lett*., **81** [3] 427–9 (2002).
[47]L. Q. Chen and J. Shen, "Applications of Semi-Implicit Fourier-Spectral Method to Phase Field Equations," *Comp. Phys. Commun*., **108** [2–3] 147–58 (1998).
[48]Y. L. Li, L. E. Cross, and L. Q. Chen, "A Phenomenological Thermodynamic Potential for $BaTiO_3$ Single Crystals," *J. Appl. Phys*., **98**, 064101 (2005).
[49]Y. L. Li, S. Y. Hu, D. Tenne, A. Soukiassian, D. G. Schlom, X. X. Xi, K. J. Choi, C. B. Eom, A. Saxena, T. Lookman, Q. X. Jia, and L. Q. Chen, "Prediction of Ferroelectricity in $BaTiO_3/SrTiO_3$ Superlattices with Domains," *Appl. Phys. Lett*., **91**, 112914 (2007).
[50]D. A. Tenne, A. Bruchhausen, N. D. Lanzillotti-Kimura, A. Fainstein, R. S. Katiyar, A. Cantarero, A. Soukiassian, V. Vaithyanathan, J. H. Haeni, W. Tian, D. G. Schlom, K. J. Choi, D. M. Kim, C.-B. Eom, H. P. Sun, X. Q. Pan, Y. L. Li, L. Q. Chen, Q. X. Jia, S. M. Nakhmanson, K. M. Rabe, and X. X. Xi, "Nanoscale Ferroelectricity in $BaTiO_3/SrTiO_3$ Superlattices Probed by Ultraviolet Raman Spectroscopy," *Science*, **313**, 1614 (2006).
[51]N. A. Pertsev, A. K. Tagantsev, and N. Setter, "Phase Transitions and Strain-Induced Ferroelectricity in $SrTiO_3$ Epitaxial Thin Films," *Phys. Rev. B*, **61** [2] R825 (2000).
[52]S. Rios, A. Ruediger, A. Q. Jiang, J. F. Scott, H. Lu, and Z. Chen, "Orthorhombic Strontium Titanate in $BaTiO_3$–$SrTiO_3$ Superlattices," *J. Phys. Condensed Matter*, **15** [21] L305–9 (2003).
[53]A. Vasudevarao, A. Kumar, L. Tian, J. H. Haeni, Y. L. Li, C. J. Eklund, Q. X. Jia, R. Uecker, P. Reiche, K. M. Rabe, L. Q. Chen, D. G. Schlom, and V. Gopalan, "Multiferroic Domain Dynamics in Strained Strontium Titanate," *Phys. Rev. Lett*., **97**, 257602 (2006).
[54]Y. L. Li, L. Q. Chen, G. Asayama, D. G. Schlom, M. A. Zurbuchen, and S. K. Streiffer, "Ferroelectric Domain Structures in $SrBi_2Nb_2O_9$ Epitaxial Thin Films: Electron Microscopy and Phase-Field Simulations," *J. Appl. Phys*., **95** [11] 6332–40 (2004).
[55]J. X. Zhang, Y. L. Li, Y. Wang, Z. K. Liu, L. Q. Chen, Y. H. Chu, F. Zavaliche, and R. Ramesh, "Effect of Substrate-Induced Strains on the Spontaneous Polarization of Epitaxial $BiFeO_3$ Thin Films," *J. Appl. Phys*., **101** [11] (2007).
[56]Y. H. Chu, M. P. Cruz, C. H. Yang, L. W. Martin, P. L. Yang, J. X. Zhang, K. Lee, P. Yu, L. Q. Chen, and R. Ramesh, "Domain Control in Multiferroic $BiFeO_3$ through Substrate Vicinality," *Adv. Mater*., **19**, 2662–6 (2007).
[57]M. P. Cruz, Y. H. Chu, J. X. Zhang, F. P. Zavaliche, L. Yang, P. Shafer, L. Q. Chen, and R. Ramesh, "Control of the Ferroelastic Switching Mechanism in $BiFeO_3$ Films," *Phys. Rev. Lett*., **99**, 217601 (2007).
[58]J. Slutsker, I. Levin, J. H. Li, A. Artemev, and A. L. Roytburd, "Effect of Elastic Interactions on the Self-Assembly of Multiferroic Nanostructures in Epitaxial Films," *Phys. Rev. B*, **73**, 184127 (2006).
[59]J. X. Zhang, Y. L. Li, D. G. Schlom, L. Q. Chen, F. Zavaliche, R. Ramesh, and Q. X. Jia, "Phase-Field Model for Epitaxial Ferroelectric and Magnetic Nanocomposite Thin Films," *Appl. Phys. Lett*., **90**, 052909 (2007).
[60]B. J. Roriguez, S. V. Kalinin, S. Jesse, Y. H. Chu, T. Zhao, R. Ramesh, S. Choudhury, L. Q. Chen, E. A. Eliseev, and A. N. Morozovska, "Self-Consistent Spectroscopic Measurements of Single Domain Switching in Ferroelectric Materials: Nucleation Mechanism and Domain Growth", *Proceedings of the National Academy of Sciences*, 2007. accepted.
[61]S. Jesse, J. Rodriguez, A. P. Baddorf, I. Vrejoiu, D. Hesse, M. Alexe, E. A. Eliseev, A. N. Morozovska, J. X. Zhang, S. Choudhury, L. Q. Chen, and S. V. Kalinin, "Direct Imaging of Spatial and Energy Distribution of Nucleation Centers in Ferroelectric Materials: 50 Years After Landauer," *Nat. Mater*., **7**, 209–15 (2008).
[62]L. Tian, N. Ogadawa, S. Choudhury, A. Vasudevarao, P. Capek, V. Dierolf, A. N. Morozovska, E. A. Eliseev, L. Q. Chen, Y. Cho, S. V. Kalinin, and V. Gopalan, "Domain Wall Width and Coercive Field in Ferroelectrics," *Phys. Rev. Lett*. (2007), Submitted.
[63]W. Zhang and K. Bhattacharya, "A Computational Model of Ferroelectric Domains. Part II: Grain Boundaries and Defect Pinning," *Acta Materialia*, **53** [1] 199–209 (2005).
[64]S. Choudhury, Y. L. Li, C. Krill, and L. Q. Chen, "Effect of Grain Orientation and Grain Size on Ferroelectric Domain Switching and Evolution: Phase Field Simulations," *Acta Materialia*, **55** [4] 1415–26 (2007).
[65]S. Choudhury, Y. L. Li, C. E. Krill, and L. Q. Chen, "Phase-Field Simulation of Polarization Switching and Domain Evolution in Ferroelectric Polycrystals," *Acta Materialia*, **53** [20] 5313–21 (2005).

[66]S. Y. Hu, Y. L. Li, and L. Q. Chen, "Effect of Interfacial Dislocations on Ferroelectric Phase Stability and Domain Morphology in a Thin Film—a Phase-Field Model," *J. Appl. Phys.*, **94** [4] 2542–7 (2003).

[67]Y. Zheng, B. Wang, and C. H. Woo, "Effects of Interface Dislocations on Properties of Ferroelectric Thin Films," *J. Mech. Phys. Solids*, **55** [8] 1661–76 (2007).

[68]H. L. Hu, Y. L. Li, S. Choudhury, A. Saxena, T. Lookman, M. Baskes, Q. X. Jia, D. G. Schlom, and L. Q. Chen, "Influence of Interfacial Dislocations on Hysteresis Loop of Ferroelectric Materials," *Appl. Phys. Lett*. (2007), Submitted.

[69]S. Choudhury, Y. L. Li, and L. Q. Chen, "Tailoring Domain Switching Behavior in Barium Titanate Thin Films Using Substrate Constraint," *Appl. Phys. Lett*. (2007), in press.

[70]Y. Xiao, V. B. Shenoy, and K. Bhattacharya, "Depletion Layers and Domain Walls in Semiconducting Ferroelectric Thin Films," *Phys. Rev. Lett*., **95** [24] (2005).

[71]J. X. Zhang, R. Wu, S. Choudhury, and L. Q. Chen, "Three-dimensional Phase-Field Simulations of Domain Structures in Ferroelectric Islands," *Appl. Phys. Lett*., 2007, in press.

[72]J. X. Zhang and L. Q. Chen, "Piezoelectricity of Ferroelectric Islands, unpublished, 2007.

[73]J. Wang and T. Y. Zhang, "Phase Field Simulations of Polarization Switching-Induced Toughening in Ferroelectric Eramics," *Acta Materialia*, **55** [7] 2465–77 (2007).

[74]Y. C. Song, A. K. Soh, and Y. Ni, "Phase Field Simulation of Crack Tip Domain Switching in Ferroelectrics," *J. Phys. D-Appl. Phys*., **40** [4] 1175–82 (2007).□